Chemistry Africa (2022) 5:359–373
https://doi.org/10.1007/s42250-021-00308-x

ORIGINAL ARTICLE

Dehydrate Sewage Sludge as an Efficient Adsorbent for Malachite Green Removal in Textile Wastewater: Experimental and Theoretical Studies

Youssef Aoulad El hadj Ali[1] · Abdoulaye Demba N'diaye[2] · Mohammadi Ahrouch[3,4] · El Hassan Sakar[5] · Anas Raklami[6] · Abdellatif Ait Lahcen[7] · Mostafa Stitou[1]

Received: 8 October 2021 / Accepted: 21 December 2021 / Published online: 21 January 2022

Abstract

We present in this study a simple approach on the application of dried dewatered sewage sludge (D@DSS) generated from a local wastewater treatment plant (WWTP). The D@DSS can be considered as an alternative friendly and cost-effective adsorbent for malachite green (MG) dye removal from an aqueous solution using batch systems. This procedure did not require any modification of the adsorbent characteristics. D@DSS demonstrated an excellent retention capacity for MG at synthetic solutions, and in industrial wastewater. Moreover, the selectivity study of the adsorbent was performed against Methylene Blue and Red Congo shows better capability of this adsorbent towards cationic dyes. The D@DSS adsorbent characterization was carried-out using SEM, FTIR, Zeta potential, XRD and ICP. The results confirmed a rough and charged surface of the adsorbent with the presence of specific functional groups. The adsorption process fits well with the Jovanovic model isotherm and was adhered to the pseudo-second order kinetics. The process conditions were optimized using the response surface methodology, resulting in q_e (78.10 mg g^{-1}) for different values of the input variables, including pH (10), ionic strength (0.015 mg g^{-1}), initial concentration (150 mg g^{-1}), temperature (37.29 °C),contact time (58.25 min), adsorbent dose (0.05 g) and particle size (0.203 mm). Hence, the proposed D@DSS can be effectively applied as a low-cost adsorbent for MG elimination from different contaminated water samples and can be easily extended to remove other cationic dyes.

Keywords Dehydrate sewage sludge · Adsorption · Malachite green · Isotherm · Kinetic · Modelling study

✉ Youssef Aoulad El hadj Ali
aouladelhadjali@uae.ac.ma

✉ Mohammadi Ahrouch
ahrouch.mohammadi@uca.es

[1] Laboratoire de L'Eau, les Etudes et les Analyses Environnementales, Département de Chimie, Faculté des Sciences, Université Abdelmalek Essaadi, Mhannech II, BP 2121, 93002 Tétouan, Morocco

[2] Laboratoire de Chimie, Service de Toxicologie et de Contrôle de Qualité, Institut National de Recherches en Santé Publique, BP 695, Nouakchott, Mauritanie

[3] Laboratoire Matériaux et Systèmes Interfaciaux LMSI, Faculté des Sciences, Université Abdelmalek Essaadi, Mhannech II, BP 2121, 93002 Tétouan, Morocco

[4] Departamento C.M., I.M. y Química Inorgánica, Universidad de Cádiz, 11510 Puerto Real, Spain

[5] Department of Biology, Faculty of Sciences of Tetuan, Abdelmalek Essaâdi University, Mhannech II, 93002 Tetuan, Morocco

[6] Laboratory of Microbial Biotechnologies, Agrosciences and Environment, Faculty of Sciences Semlalia, Cadi Ayyad University, PO Box 2390, Marrakech, Morocco

[7] Advanced Membranes and Porous Materials Center, King Abdullah University of Science and Technology (KAUST), Thuwal, Saudi Arabia

1 Introduction

Water is considered an essential for the economic development of the human civilization due to its use in many sectors, especially in industry and agriculture. This vital resource is well known for its great fragility. The main sources of its contamination are urban, agricultural, and industrial. Recently, the rapid increase of the industrialization involves an increase in the volume of dyes generated by these sectors, which, may lead to serious environmental threats. In such context, authorities and environmental activists are on the alert to deal with this problem. Malachite green (MG) as cationic dye is mainly used in the textile, silk, dyeing wool, paper, leather, cotton as well as a biocide and disinfectant [1, 2]. Nowadays, treating MG dye contaminated wastewater is becoming an urgent environmental issue due to its toxicity that is creating a serious hazard to the aquatic system and to the human health [3, 4].

Due to the tightening of legislations related to industrial wastewater discharge, it is becoming mandatory to treat the MG used in industry as a raw material before discharging it into the environment. Many treatment techniques have been reported for the MG removal including electrochemical degradation [5], oxidation processes, [6] and photocatalytic degradation [7]. However, these methods present some drawbacks such as their high-cost and less efficiency to treat a plethora of dye wastewater. Recently, the adsorption method is widely used to remove pollutants from aqueous medium thanks to its outstanding features such as high efficiency, simplicity of design, and cost-effectiveness [8, 9]. In fact, activated carbon is the most commonly used material in adsorption [9]. However, high cost to prepare the activated carbon limits its application on a large scale [10, 11]. To overcome this limitation, the recent research studies focus on finding/exploring natural adsorbents that might be used as potential alternatives to the activated carbon [12]. In this context, natural adsorbents are favorized due to their biodegradability, non-toxic nature, cost-effectiveness, and eco-friendly features [13]. As a result, several low-cost adsorbents for the retention of MG have been reported [15, 19]. Cheng et al. [20] have reported the adsorption of MG using two adsorbents produced from sewage sludge (native anaerobic granular sludge and autoclaving anaerobic granular sludge that was prepared at 116 °C and 110 kPa for 30 min). The kinetic studies have been performed using pseudo-first order (PFO) and pseudo-second order (PSO). Moreover, conventional models of Langmuir and Freundlich isotherms adsorption were used to investigate the adsorption data, then they found that the two adsorbents used have a higher adsorption capacity towards the removal of MG [20].

In this research work, the D@DSS was selected to investigate its potential use as an effecient adsorbent for MG dye removal in textile contaminated wastewater. Herein, the influence of different operating parameters on the MG adsorption onto D@DSS have been studied and optimized using response surface methodology. Indeed, the adsorbent dosage, the initial dye concentration, the effect of contact time, and ionic strength have been investigated. Thermodynamics, kinetics, and isotherm studies were carried out to study the adsorption process efficiency. Also, the adsorbent was tested with two categories of dyes (Congo Red, Methylene Bleu). Lastly, the D@DSS was applied to remove MG in real wastewater, which confirm the efficiency and reusability of the adsorbent on a large scale.

2 Materials and Methods

2.1 Preparation of Malachite Green Adsorbate

In this study, MG was chosen as a model dye because it is commonly used in the textile industry and in laboratory experiments, and it is highly toxic to aquatic life. The MG stock solution was prepared by dissolving 1 g in 1 L of deionized water (DI). All MG diluted solutions were prepared using DI and were used to develop the standard curves using the Spectrophotometer UV1800 Ray Leigh. The initial pH was adjusted using HCl or NaOH solutions (0.1 mol L^{-1}). pH measurements were performed with PHSJ-3F pH meter.

2.2 Preparation and Characterization of D@DSS Adsorbent

Dehydrate sewage sludge (D@DSS) samples were collected from Tamuda bay domestic WWTP (Mdiq-Fnideq/Morocco).the sampling process carried out by taken about 7 L of sample in polyethylene bottles, the raw material was dough a fresh and dark black colored. It was first dried at 40 °C in furnace for 24 h, then crushed in a grinder and analyzed by particle size analysis (Endecotts Ltd, Lombard Road, London, SW, 93BR England, Telex: 929395) in order to obtain fine particles characterized by a diameter between 0.2 and 2.5 mm. Further, the obtained D@DSS powder was packed into small boxes and stored in a desiccator containing silica gel until further use [21]. Then, to characterize the adsorbent, Fourier transformed infrared (FTIR) analyses, were performed using Thermo Vertex 70 spectrophotometer before and after adsorption.1 mg grounded D@DSS was mixed with 200 mg of potassium bromide. Then, a high pressure (10 kg cm^{-3}) was used to prepare a pellet from the sample. This sample was tested at 4 cm^{-1} resolutions (100 scans) in the spectral reflectance range of 4000–400 cm^{-1}. Scanning electron microscopy (SEM) prior and post adsorption was used to determine the morphological characteristics of the D@DSS adsorbent. Hence, using the acceleration

voltage of 10 kV was acquired using a "Hirox SEM. The surface charge of the adsorbent was measured using zeta potential instrument (Malvern zetameter model Zetasizer Nano Z). Inductively ICP and X-ray fluorescence (Siemens D5000 automatic diffractometer) were used to determine the chemical composition of D@DSS.

2.3 Batch Adsorption Studies

The adsorption of MG using D@DSS was conducted in batch experiments. The effect of process conditions, mass effect (0.05–1.5 g), contact time (0–90 min), pH effect (2–12), initial concentration, (5–50 mg L^{-1}) and ionic strength (0.005–1 mol L^{-1}) were evaluated. To assess the adsorption properties of the D@DSS, the adsorption isotherms were conducted by changing the initial MG concentrations from 5 to 150 mg L^{-1}. Once the experiment done, the obtained solution was centrifuged, and the MG amount was determined from the resultant supernatant which was measured using a Spectrophotometer regulated at λ equal to 618 nm. The MG amount adsorbed at equilibrium time q_e (mg g^{-1}) and the percentage of the MG removal (%) are expressed as follow:

$$q_e = \frac{(C_\mathrm{i} - C_\mathrm{e})V}{m} \tag{1}$$

$$\%Removal = \frac{(C_\mathrm{i} - C_\mathrm{e})}{C_\mathrm{i}} \times 100 \tag{2}$$

where q_e is the MG concentration adsorbed by D@DSS (mg g^{-1}), C_i is the initial MG concentration (mg L^{-1}); C_e is the MG concentration at equilibrium (mg L^{-1}); V is the solution volume (L) and m is the mass of the D@DSS used (g). All batch experiments were performed in triplicate.

The kinetics of adsorption allow a better understanding of the adsorption and kinetic mechanism, which control the adsorption process and estimates the physical or chemical adsorption. Two adsorption models, PFO and PSO were used to investigate the adsorption data. The nonlinear regression kinetics PFO and PSO models expressed as follow [22, 23]:

$$q_t = q_e(1 - \exp^{-k_1 t}) \tag{3}$$

$$q_t = \frac{k_2 q_e^2 t}{1 + k_2 q_e t} \tag{4}$$

where q_t is the adsorbed amount of MG adsorbed of D@DSS (mg g^{-1}) at time t, k_1 (L min^{-1}) is the PFO rate constant, k_2 (mg g^{-1} min^{-1}) is the PSO rate constant for adsorption, q_e (mg g^{-1}) the amount of MG adsorbed at equilibrium and t is the contact time (min).

To evaluate the adsorption process efficiency, Langmuir, Freundlich and Jovanovic models, were used. The Langmuir model is defined as a monolayer adsorption upon the homogeneous surface of the adsorbent and follows the equation below [22]:

$$q_e = \frac{q_m K_L C_e}{1 + K_L C_e} \tag{5}$$

where q_e is the adsorbed amount of MG per unit mass of D@DSS adsorbent (mg g^{-1}), k_L is the Langmuir constant related to the adsorption capacity (L g^{-1}), C_e is the equilibrium concentration of MG (mg L^{-1}), q_m is the maximum adsorption capacity per unit mass of D@DSS adsorbent (mg g^{-1}).

Freundlich model suggests a multilayer adsorption upon the heterogeneous surface of sorbent material and presented as Eq. (6) [24]:

$$q_e = K_F C_e^{1/n} \tag{6}$$

where 1/n and K_F (mg g^{-1}) (L $mg^{-1})^n$ are the Freundlich constants related to adsorption capacity and adsorption intensity, respectively.

The model of Jovanovic presented in Eq. (7) has some similar features as the one considered by Langmuir with small difference, that Jovanovic model suggests the possibility of mechanical contact between the adsorbing and the desorbing molecules [25].

$$q_e = q_m\left(1 - e^{-K_J C_e}\right) \tag{7}$$

where, q_m (mg g^{-1}) is the Jovanovic maximum adsorption capacity and K_J (L mg^{-1}) is the Jovanovich isotherm constant.

3 Results and Discussion

3.1 Characterization of D@DSS Adsorbent

Regarding the surface chemistry quantification, the results of the total surface acidity of 3.864 meq g^{-1} and total surface basicity of 1.71 meq g^{-1} confirmed that the studied D@DSS predominantly possess an acidic nature. The Beumer-Emmet-Teller (BET) characterization technique confirmed the surface area for D@DSS adsorbent to be ranging from 24.42 to 18.00 m^2 g^{-1} for a particles size varying from 0.4 to 2.5 mm (Table S1, supplementary information), without any chemical or thermal process is satisfactory [21].

The chemical composition of the used adsorbent was performed to prevent some toxic elements like heavy metals during its application in aqueous solutions. The analysis of heavy metals, total hydrocarbons, and nitrogen in the D@DSS is presented in Table 1. The obtained results showed that the sludge has trace amounts of heavy metals, making it safe and suitable to use it as an adsorbent in aqueous solutions.

Therefore, the examination of the results obtained by X-ray fluorescence shows that the D@DSS is rich in calcite 40.8%, iron 25.08% and in silica 11.9% (Fig. 1A). Table 1 and Fig. 1A indicate that D@DSS can be used as a natural, low-cost substitute for some commercial adsorbents.

Figure 1B shows FTIR spectra of D@DSS before and after the MG adsorption. The results obtained for D@DSS before adsorption showed peaks located at 3694, 3324, 2921, 2852, 1659,1548, 1436, 1031, 536, and 467 cm^{-1} (Fig. 1B). The bands at 2852 cm^{-1} and 2921 cm^{-1} can be attributed to the C–H in methyl and methylene groups, respectively. The band at 1659 cm^{-1} related to C=O stretching of carboxyl groups. The most intense bands are perfectly observed at 1031 cm^{-1} in the spectra of D@DSS can be attributed to Si–O–Si or Si–O–C structures, which is associated to the presence of silicon in the sewage sludge as confirmed by the FL-X-ray spectra (Fig. 1A). After MG adsorption, the slight shift of peaks was at 3700, 3317, 2929, 2850, 1650, 1439 and 1430 cm^{-1} (Fig. 1B). A slight shift of frequency and a slighter decrease in intensity of some peaks could be attributed to MG ions

Table 1 Chemical composition of D@DSS before MG adsorption

Hg	Cd	As	Cr T	Pb	CN	THC	TkN	NH_4	NO_3	NGL
mg/kg (dried base)										
0.548	0.893	0.45	27.6	43.9	11.6	3201	52.3	5.96	0.0003	57.9
Limit values according to the Moroccan legislation (mg/kg dried base)										
10	10	–	1000	800	–	–	–	–	–	–

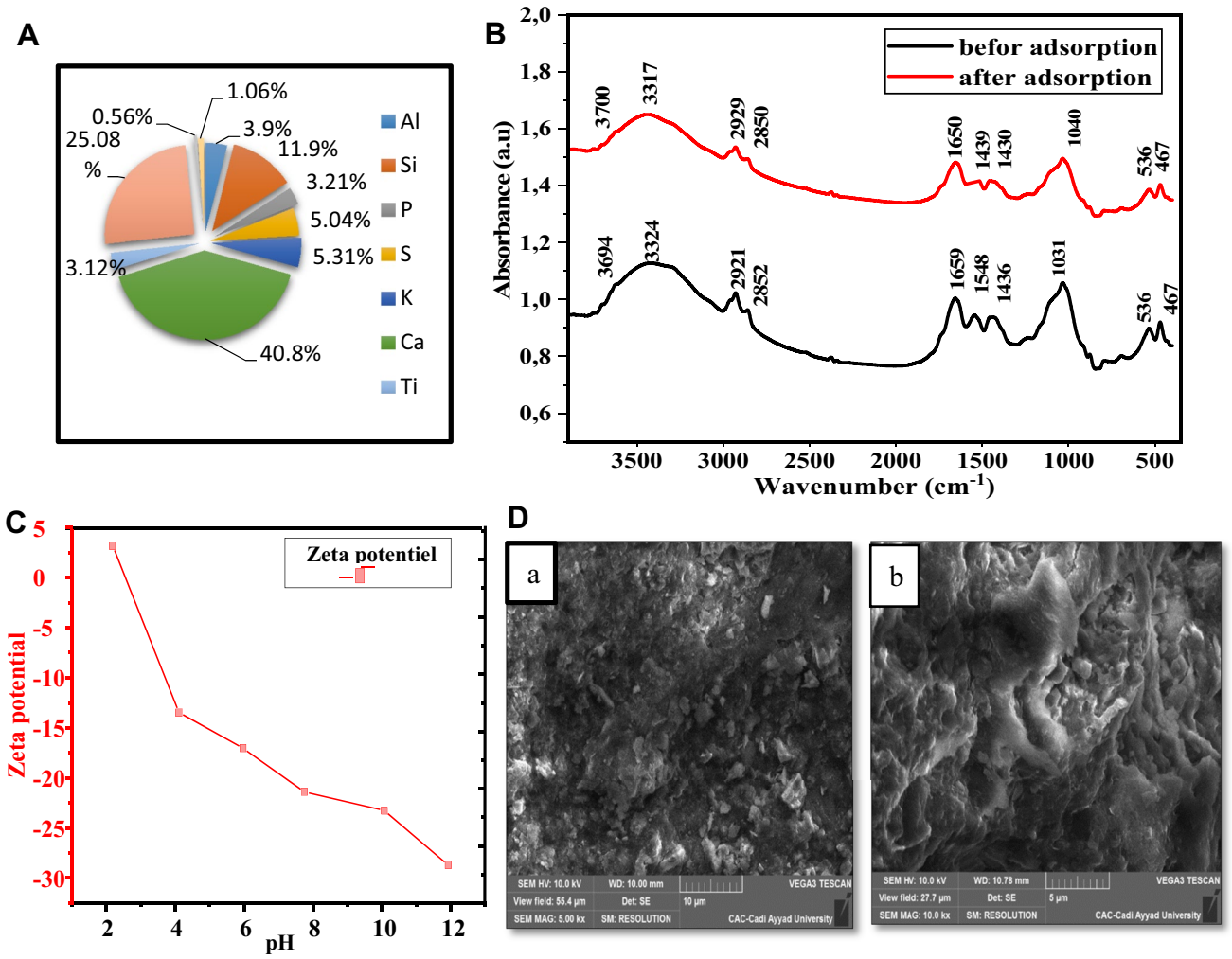

Fig. 1 **A** Major elements in (%) present in the D@DDS Before MG adsorption. **B** FTIR spectra of D@DSS adsorbent before and after MG adsorption. **C** Zeta potential of D@DDS samples. **D**. Typical SEM micrograph of D@DSS particle (100 magnification): (a) before MG ad

adsorbed onto D@DSS adsorbent. The FTIR spectroscopic study after adsorption confirmed that the MG has a binding ability with the surface of D@DSS adsorbent.

Figure 1C shows that the zeta potential of D@DSS at the pH range from 3 to 12, is negatively charged. Thus, this suggests that the D@DSS could be used to remove cationic dyes like MG in this pH mediums.

According to (Fig. 1Da), the D@DSS before MG adsorption process exhibited an irregular surface with considerable rough and porous layers that offer high adsorption capability for the adsorption of dye molecules [26]. Therefore, the SEM image of D@DSS after the adsorption of MG (Fig. 1Db) approves the smoother surface characteristics with apparent reduced pore structures, showing the high uptake and entrapment of MG by the accessible porous sites. Figure 1Db proves the entrapment of MG onto D@DSS that can be attributed to the presence of carboxylic group within D@DSS, as evidenced by the FTIR spectral (Fig. 1B), which plays the role of active sites for the MG adsorption.

3.2 *Optimizing Using Response Surface Methodology (RSM)*

Several statistical experimental designs have been considered as useful approaches for the process variables optimization. RSM is widely used, especially when a few significant independent variables are involved in the optimization process [27, 28]. In such context, Box–Behnken design (BBD) is an independent, rotatable, or approximately rotatable quadratic design where the midpoints of the edges of the process space and at the center is the treatment combinations. RSM is a three steps approach: (1) designing then performing experiments; (2) modeling response surface using regression and (3) optimizing. The aim of RSM is to obtain the optimal conditions that satisfy the operating specifications [29]. It is noteworthy that RSM is an effective and low-cost method for bioprocess modeling and optimizing since it allows the identification of interactions between investigated variables and therefore running few possible experiments. In this study, the experimental design matrix obtained from the BBD model is shown in Table S2, Supplementary information. The adsorbent amount was taken as the response of the design experiments. A total of 64 experiments were needed to calculate coefficients of second-order polynomial equation which were fitted in experimental data. The optimization was carried out using STATGRAPHICS package version XVII (Statpoint Technologies, Inc., Virginia, USA).

Table 2 Experimental range and level of input (independent) variables: pH, ionic salt (IS), initial

Input variables, nomenclature, range and levels (coded)	− 1	0	+ 1
pH	02	06	12
Ionic strength (IS, mg/L)	0.005	0.105	0.100
Initial concentration (Ci, mg/L)	005	155	150
Temperature (T, °C)	25	75	50
Time (Ti, min)	05	85	80
Adsorbent dose (AD, g)	0.05	1.55	1.50
Particle size (PS, mm)	0.2	2.7	2.5

In our work, optimization was made using seven independent variables. Table 2 summarizes these variables, their ranges, and levels. Experimental design for the seven investigated input variables and observed response is presented in Table S3, Supplementary information.

When a fitting of the interaction terms to the obtained experimental data according to the Box–Behnken model experiment, a second-order polynomial model can be written as presented in Eq. (8)

$$Y = a_0 + \sum a_0 X_i + \sum a_{ii} X_i^2 + \sum a_{ij} X_i X_j \tag{8}$$

where Y is the amount adsorbed, a_0 is the offset term, a_i is the first-order main effect, a_{ii} is the second-order main effect and a_{ij} is the interaction effect. The coefficient of determination (R^2) and the analysis of variance were computed to test the performance of fit of the model.

Equation (9) expressed the quadratic equation model for predicting the optimal point:

$$Y = b_0 + \sum_{i}^{n} b_i X_n + \sum_{i}^{n} d_i X_i^2 \pm \varepsilon \tag{9}$$

Analyzing the RSM contour plots and solving the regression equation allow obtaining the optimum values of the input variables [30]. According to our outcomes, the following quadratic model presented below was used to describe the relationship between the response and the input variables:

$$\begin{aligned} q_e &= 17.94 + 0.19\mathrm{pH} - 2.22\mathrm{IS} + 0.27\mathrm{Ci} + 1.19\mathrm{T} + 0.01\mathrm{T_i} - 3.22\mathrm{AD} - 0.08\mathrm{PS} \\ &\quad - 8.82 \cdot 10^{-3}\mathrm{pH}^2 + 4.35 \cdot 10^{-6}\mathrm{pHPS} + 17.89\mathrm{IS}^2 + 3.63 \cdot 10^{-6}\mathrm{ISC_i} - 3.63 \cdot 10^{-4}\mathrm{ISAD} \\ &\quad - 1.82 \cdot 10^{-4}\mathrm{C_i^2} + 1.38 \cdot 10^{-8}\mathrm{Ci} * \mathrm{T} + 2.38 \cdot 10^{-7}\mathrm{C_iAD} + 1.50 \cdot 10^{-7}\mathrm{C_iPS} - 1.59 \cdot 10^{-2}\mathrm{T}^2 \\ &\quad - 8.03 \cdot 10^{-5}\mathrm{TT_i} + 4.16 \cdot 10^{-3}\mathrm{TAD} + 870 \cdot 10^{-7}\mathrm{TPS} \\ &\quad - 6.25 \cdot 10^{-5}\mathrm{T_i^2} + 1.39 \cdot 10^{-3}\mathrm{T_iAD} + 1.14\mathrm{AD}^2 + 2.24 \cdot 10^{-2}\mathrm{PS}^2. \end{aligned}$$

3.3 Analysis of Variance

Combined analyses of variance for the response variable (q_e, mg/g) are presented in Table 3. As it can be seen, except IS (ionic strength) investigated factors impacted significantly (at least at 5%) on Qe. The mathematical model had good performance since R^2% exceed 99%. Regarding optimizing (maximizing) qe using RSM, as summarized in Table 4, optimum value of qe (78.105 mg/g) was reached under various values of input variables: pH (10), IS (0.015), Ci (150), T (37.29), Ti (58.25), AD (0.05), and PS (0.203).Typically in order that a model is repeatable, the coefficient of variance

Table 4 Optimized response q_e under various experiment conditions according to Box–Behnken approach

Factor	Low	High	Optimum
pH	2.0	12.0	10.0
IS	0.005	0.1	0.0145315
Ci	5.0	150.0	150.0
T	25.0	50.0	37.2874
Ti	5.0	80.0	58.2493
AD	0.05	1.5	0.05
PS	0.2	2.5	0.202967

Table 3 Combined analyses of variance for qe. Df = degree of freedom

Source of variation	Sum of squares	Df	Mean square	F-ratio	P-value
A:pH	2.98159	1	2.98159	1031.59	0.0000
B:IS	0.00636027	1	0.00636027	2.20	0.1491
C:Ci	7527.98	1	7527.98	2,604,585.33	0.0000
D:T	0.0422688	1	0.0422688	14.62	0.0007
E:Ti	0.345912	1	0.345912	119.68	0.0000
F:AD	19.5009	1	19.5009	6747.06	0.0000
G:PS	0.0185315	1	0.0185315	6.41	0.0172
AA	0.699616	1	0.699616	242.06	0.0000
AB	0.0	1	0.0	0.00	1.0000
AC	0.0	1	0.0	0.00	1.0000
AD	0.0	1	0.0	0.00	1.0000
AE	0.0	1	0.0	0.00	1.0000
AF	0.0	1	0.0	0.00	1.0000
AG	$5.E^{-9}$	1	$5.E^{-9}$	0.00	0.9990
BB	0.0234595	1	0.0234595	8.12	0.0081
BC	$1.25E^{-9}$	1	$1.25E^{-9}$	0.00	0.9995
BD	0.0	1	0.0	0.00	1.0000
BE	0.0	1	0.0	0.00	1.0000
BF	$1.25E^{-9}$	1	$1.25E^{-9}$	0.00	0.9995
BG	0.0	1	0.0	0.00	1.0000
CC	13.1884	1	13.1884	4563.02	0.0000
CD	$1.25E^{-9}$	1	$1.25E^{-9}$	0.00	0.9995
CE	0.0	1	0.0	0.00	1.0000
CF	$1.25E^{-9}$	1	$1.25E^{-9}$	0.00	0.9995
CG	$1.25E^{-9}$	1	$1.25E^{-9}$	0.00	0.9995
DD	89.2532	1	89.2532	30,880.49	0.0000
DE	0.0113477	1	0.0113477	3.93	0.0574
DF	0.0113477	1	0.0113477	3.93	0.0574
DG	$1.25E^{-9}$	1	$1.25E^{-9}$	0.00	0.9995
EE	0.111355	1	0.111355	38.53	0.0000
EF	0.0113477	1	0.0113477	3.93	0.0574
EG	0.0	1	0.0	0.00	1.0000
FF	5.13089	1	5.13089	1775.22	0.0000
FG	0.0	1	0.0	0.00	1.0000
GG	0.0126274	1	0.0126274	4.37	0.0458
Total error	0.0809278	28	0.00289028		
Total (corr.)	7661.92	63			

(CV%) should not be greater than 10%. The data obtained in this study confirmed that the calculated CV value of the model is 3.50% demonstrating the repeatability of the model.

The obtained model was evaluated via two indicators: the percentage absolute error of deviation (AED) and the regression coefficient (R^2). AED was calculated using the following equation:

$$\mathrm{AED}(\%) = 100/\mathrm{N} \cdot \sum \left| (\mathrm{Y}_{\mathrm{exp}} - \mathrm{Y}_{\mathrm{theo}})/\mathrm{Y}_{\mathrm{exp}} \right|. \quad (10)$$

where Y_{exp} are the experimental responses and Y_{theo} are the theotrical responses. And N is the number of point at which measurements were carried out.

The obtained model was valid since the AED % = 0.237 is lower than 10% and R^2 99.99% > 0.7.

To plot the response surface, only significant input variables were considered ($p < 0.05$). The combined effects of these variables on the response variable are presented in Fig S1, Supplementary information. Effects of pH combined separately with the remaining significant factors are plotted in Fig S1. A–E, Supplementary information, the greatest values of $q_e$were obtained with higher values of pH (10) combined with Ci (150 mg/L), T (30 °C), Ti (60 min), AD (0.05 g), and PS (0.2 mm). When combining Ci with other input variables (Fig S1. F–I, Supplementary information), it seems that q_e increased gradually to reach its great values at Ci (150 mg/L), T (30 °C), Ti (60 min), AD (0.05 g), and PS (0.2 mm). Fig S1. J–L, Supplementary information presents variation of q_e as functions of T combined separately with Ti, AD, and PS. From these outcomes, no noticeable increase of q_e (around 60 mg/g) was reached at Ti (60 min), AD (0.05 g), and PS (0.2 mm). Similarly, when plotting q_e against (Ti, AD), (Ti, pH), and (AD, PS), as illustrated in (Fig S1. M–O, Supplementary information), q_e had its better values (about 60–64 mg/g) at Ti (60 min), AD (0.05 g), pH (10), and PS (0.2 mm).

3.4 Effect of D@DSS Adsorbent Mass

The adsorbent mass is a crucial parameter in adsorption studies, as it indicates the optimal dose where the maximum adsorption appears. The influence of the D@DSS amount on the adsorption efficiency was investigated and optimized. Different doses in the range 0.05–1.5 g at a fixed MG concentration (10 mg L^{-1}) for MG removal by D@DSS is indicated in (Fig. 2A). The results indicate that the increase in the adsorbent amount leads to the adsorption elimination increase, which might be due to the increase in the surface area retention [31].

However, more increase after a certain amount (q_e = 1.26 mg g^{-1}, %E = 90) does not enhance the adsorption, which might be due to the interference between binding sites of the D@DSS adsorbent at different amounts. In this context, a similar phenomenon was reported using Typha australis leaves for MG adsorption [32]. The optimal D@DSS adsorbent dose obtained is 0.7 g.

3.5 Effect of pH on the D@DSS Adsorption Efficiency

To study the influence of pH on the adsorption of MG onto D@DSS, the experiments were performed at an initial dye concentration of 10 and 30 mg L^{-1}. The amount of the adsorbed MG onto D@DSS in the pH range from 2 to 12 was shown in (Fig. 2B). The adsorption of MG over the D@DSS increased from 0.85 to 1.34 mg g^{-1} and from 2.75 to 4.14 mg g^{-1} at initial dye concentrations of 10 and 30 mg L^{-1} at 20 °C, respectively, with the increase in pH from 2 to 12. This observation may be explained as follow, at pH 2, the D@DSS surface became positively charged, making H^+ ions compete with cationic MG dye. As a result, the removal capacity is decreased due to the electrostatic repulsion force. While, at pH higher than 2, a higher amount of negatively charged OH^- are dominant on the surface of D@DSS. Thus, it enhanced the electrostatic attraction, which facilitates more MG adsorption capacity [33, 34]. The highest the pH value, the strongest the adsorption, may also be explained by the Zeta potential analyses results. Figure 1C mentions clearly that the Zeta potentials of D@DSS are increasing from pH 2 to 12. Consequently, due to the electrostatic interactions, the amount of MG adsorption on the D@DSS is increased with the increase of pH, which is in correlation with previous reports [27, 35]. Indeed, according to Parthasarathy et al. [36], this phenomenon can also be explained by: with the increasing of pH, the zwitterions of MG in aqueous medium may cause the formation of the MG aggregate, blocking the insertion into the porous structure of the adsorbent.

3.6 Effect of D@DSS Particles Size on the Adsorption Capacity

The particle size of the adsorbent usually affects the adsorption capacity. Indeed, we have studied the adsorption kinetics for the different powder granules with diameters ranging from 0.2 mm to more than 1.4 mm. As can be seen in the Fig. 2C**,** the adsorption kinetics of the dye at six different particle sizes shows that the adsorption capacity increases with decreasing particle size of D@DSS. Thus, with a given mass of D@DSS, a smaller particle size results in higher surface area Table S1, Supplementary information. Hence the number of active sites is increased. Similar results were reported for MG adsorption using Cattail leaves as a novel biosorbent [37].

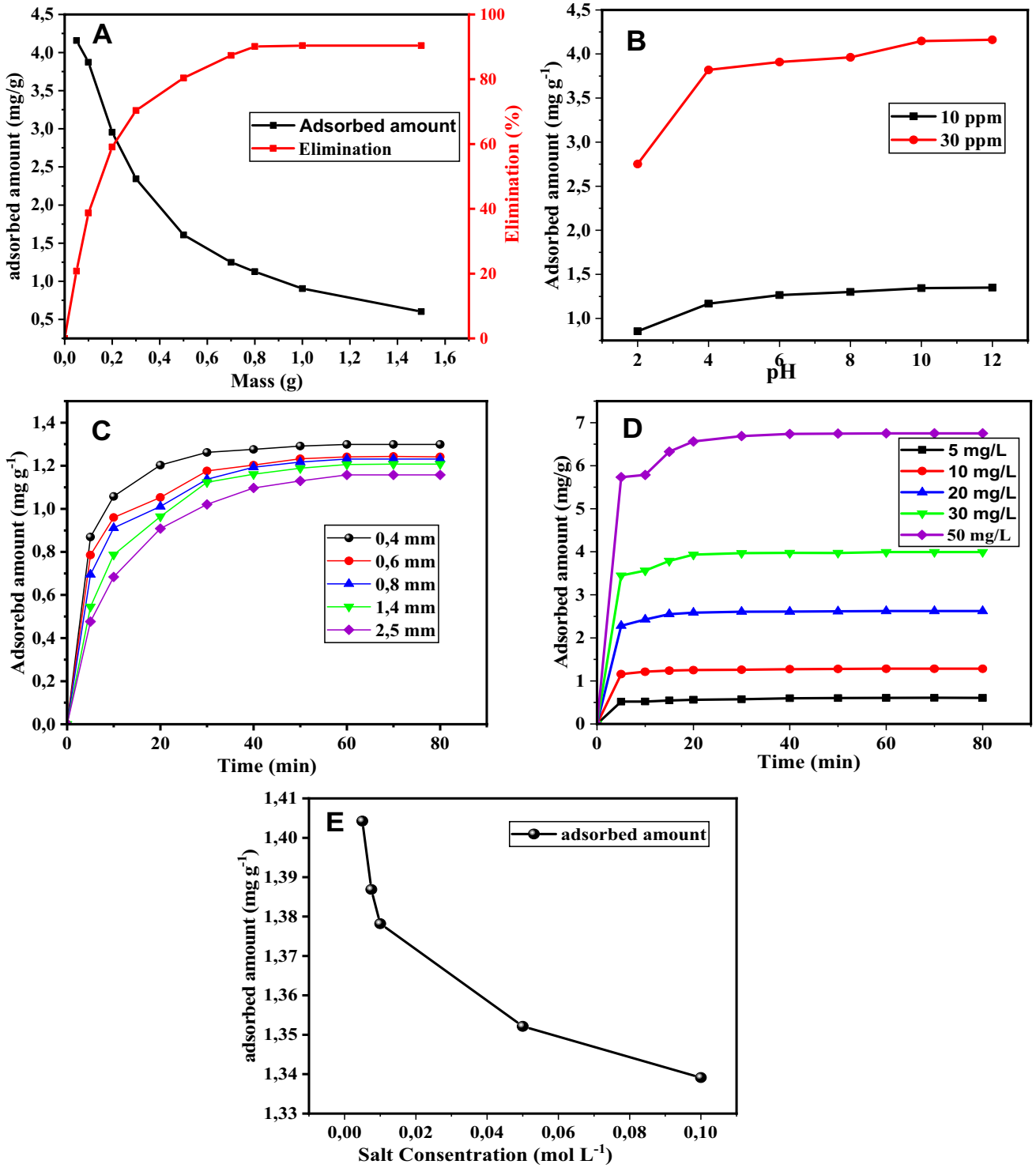

Fig. 2 **A** Effect of adsorbent dosage on the adsorption of MG by D@DSS. **B** The effect of pH on adsorption of MG onto D@DSS. **C** The effect of particle size to the adsorption rate of MG on D@DSS. **D** Kinetics of MG adsorption by D@DSS for various initial dye concentrations. **E** The effect of ionic strength on MG removal (%)

3.7 Effect of Contact Time and MG Initial Concentration

The influence of contact time and MG dye initial concentration on the adsorption uptake using D@DSS are presented in (Fig. 2D). An increase of adsorption of MG has been noticed in function of time until it reaches a saturation of D@DSS active sites. The time needed to reach equilibrium is dependent to the initial concentration of MG: in fact, about 50 min for $C_0 = 5$ mg L^{-1}, 50 min for $C_0 = 10$ mg L^{-1}, 50 min for 20 mg L^{-1}, 60 min for 30 mg L^{-1} and 60 min for 50 mg L^{-1}. The initial faster adsorption rates may also be due to the presence of a large number of active sites for adsorption and the slower adsorption rates at the end could be attributed to the saturation of the binding sites. Similar behavior was obtained for the adsorption of MG onto Neem sawdust [38].

3.8 Effect of Ionic Strength

The ionic strength of the solution is considered as an important factor that governs both electrostatic and non-electrostatic interactions between dyes and adsorbent surfaces. Hence, initial concentration of MG, contact time, temperature and adsorbent dosage were used at 10 mg L^{-1}, 80 min, 293 K and 0.7 g, respectively. The effect of the NaCl on the MG adsorption onto D@DSS is studied and the results obtained are presented in (Fig. 2E).

As can be seen in (Fig. 2E), the presence of NaCl has affected the MG retention percentage. As much as the NaCl concentration increases, the adsorption capacity of the D@DSS decreases. These results may due to the competition between MG cations and Cl^- for the active sorption sites, in correlation with published literature report [39].

3.9 Study of Adsorption Kinetics and Thermodynamic

Figure 3 shows the adsorption kinetic data for the adsorption of MG onto the D@DSS adsorbent. The Origin Software was used to calculate the adsorption kinetic parameters values and R^2 values.

The calculated values were listed in Table 5. High value of R^2 of PSO model was obtained for MG, which demonstrated that this adsorption model fits well with the adsorption data than the PFO model. These results confirm that the PSO adsorption mechanism was predominant which suggests that the chemisorption involves valence forces through sharing or exchange of electrons between the MG dye and the D@DSS. It was also observed that the PSO rate constant (k_2) was decreasing with the increased initial concentration. Similar kinetics were also obtained in adsorption of MG on Effective Micro-organisms based compost as adsorbent [40].

3.10 Thermodynamic Parameters

The study of thermodynamic parameters are useful to explain the behavior of the adsorption in terms of process equilibrium. The thermodynamic parameters indicate the effect of temperature on the adsorption process, which is determined by combining the thermodynamic Eq. (11) and van't Hoff, which allows realizing the Eyring Eq. (12).

$$\Delta G^\circ = \Delta H^\circ - T\Delta S^\circ \tag{11}$$

$$\text{Ln ke}^\circ = -\frac{\Delta H^\circ}{RT} + \frac{\Delta S^\circ}{R} \tag{12}$$

where R is the universal gas constant (8.314 J K^{-1} mol^{-1}), T (K) is the absolute temperature, ke ° is the thermodynamic equilibrium constant, and ΔH° is the enthalpy variation and ΔS° is the entropy variation. In this study, the thermodynamics of the adsorption of MG dye on D@DSS has been studied at different temperatures, In accordance with the latest estimates of different reports [41–43], it is recommended to use Eq. (13), to calculate the equilibrium constant for the adsorption process is to obtain adsorption isotherms at different temperatures.

$$\text{ke}^\circ = \frac{1000 \cdot \text{KL} \cdot \text{molecular weight of adsorbate} \cdot [\text{adsorbate}]^\circ}{\gamma} \tag{13}$$

where K_L is the Langmuir isotherm constant, which is calculated below, [adsorbate]° is the standard concentration of the adsorbate (1 mol L^{-1}), γ is the activity coefficient which is unitary for very diluted or ideal solutions and Ke ° is the thermodynamic equilibrium constant that is dimensionless. The mean change in standard enthalpy of MG adsorption on D@DSS was calculated using (Eq. 10). The values of ΔS° and ΔH° were determined from the intercept and plot slope of ln (Ke°) versus 1/T (Fig. S2 Supplementary information). The thermodynamic adsorption parameters of MG onto D@DSS were calculated from the obtained experimental data at 293, 303, 313 and 323 K, are listed in Table 6. As presented in Table 6, the values of ΔG° for the MG adsorption were − 70.52, − 71.52, − 71.98 and − 72.71 kJ mol^{-1} at 293, 303, 313 and 323 K. At all studied temperatures, the ΔG° value is negative, indicating that the adsorption of MG onto D@DSS would follow a spontaneous and favorable trend. The ΔG° value decreased with an increase in the temperature from 293 to 323 K. This confirmed an increase in the MG adsorption with increasing temperature. Similar observations are reported by Khattri and Singh [38]. The negative value of ΔH° (− 49.12 kJ mol^{-1}) indicated the exothermic process. The negative value of ΔS° (− 73.04 J mol^{-1}) suggested a decrease in randomness at the solid/liquid interface and that the internal structure of D@DSS has not significantly changed during MG adsorption [44].

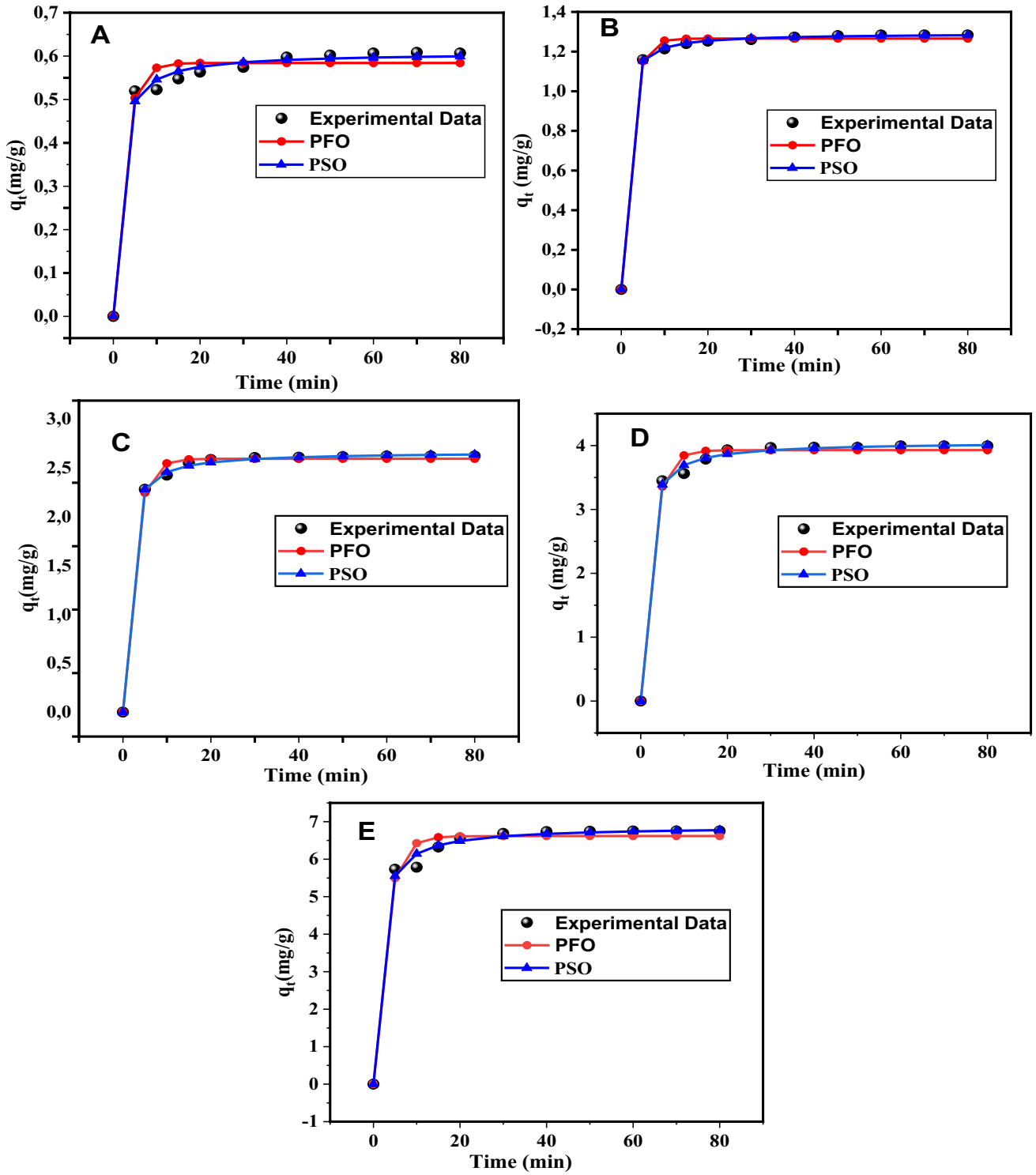

Fig. 3 PFO and PSO nonlinear for D@DSS adsorbent with initial MG concentrations of 5 (**A**), 10 (**B**), 20 (**C**), 30 (**D**) and 50 (**E**) mg L^{-1}

3.11 Adsorption Isotherm

The outcomes based on the Langmuir, Freundlich and Jovanovic isotherms are shown in Table 7. The Jovanovic model is the best model to explain the adsorption isotherm confirmed by the R^2 values. Moreover, the maximum adsorption capacity of Jovanovic is close to the maximum capacity of adsorption experiments and optimum value

Table 5 Non-linear kinetic model parameters

Model	Parameters	5 mg L^{-1}	10 mg L^{-1}	20 mg L^{-1}	30 mg L^{-1}	50 mg L^{-1}
	q_{exp}	0.602	1.280	2.62	3.99	6.75
PFO	q_e	0.584	1.265	2.595	3.929	6.616
	K_1	0.395	0.480	0.402	0.385	0.354
	R^2 (%)	97.8	99.7	99.6	99.1	98.4
PSO	q_e	0.607	1.292	2.666	4.056	6.874
	K_2	1.46	1.29	0.447	0.251	0.122
	R^2 (%)	99.3	99.9	99.9	99.8	99.5

Table 6 Thermodynamic parameters values for the adsorption of MG onto D@DSS

T (k)	ΔG° (KJ mol^{-1})	ΔH° (KJ mol^{-1})	ΔS°(J mol^{-1} K^{-1})
293	− 70.52	− 49.12	− 73.04
303	− 71.25	–	–
313	− 71.98	–	–
323	− 72.71	–	–

Table 7 Langmuir, Freundlich and Jovanovic isotherm models and constants at deferent temperature

Model	Parameters	20 °C	30 °C	40 °C	50 °C
	$q_{m,\ exp}$	66.22	65.78	68,23	65,56
Langmuir	q_m	106.2	110.3	123.2	157.6
	K_L	0.187	0.136	0.090	0.037
	R^2 (%)	98.8	96.2	99.1	99.5
Freundlich	1/n	0.63	0.65	0.69	0.77
	K_F	11.37	10.50	11.57	6.94
	R^2 (%)	95.5	91.7	98	98.7
Jovanovic	Qm	73.9	75.15	82.12	96
	Kj	0.132	0.121	0.126	0.06
	R^2 (%)	99.2	96.9	99.5	99.6

found by RSM. Thus, the Jovanovic model is a good fit for the experimental data, which shows the existence of some mechanical contact between the adsorbed and the desorbed molecules.

Moreover, as shown in (Fig. 4), the maximum adsorption capacity increases with the increase of the temperature of the solution. In addition, the temperature has a positive effect on the adsorption of MG by D@DSS, this observation confirms that the process of dye adsorption is exothermic.

3.12 Mechanism of MG Adsorption onto D@DSS

This section described the mechanism possible of the MG adsorption onto D@DSS. At pKa Below 10.3, the MG is protonated and exists in its cationic form [45], then the adsorbent negatively charged surface was approved by the zeta potential reviled that the Electrostatic attraction between MG and D@DSS is a major mechanism of adsorption. The π–π electron–donor interaction also contribute to the uptake of MG. The presence e of several benzene rings in the MG structure (polycyclic aromatic compound), which are electron-rich zones may induce a donor–acceptor relationship and a stacking effect of the MG onto the adsorbent [46, 47]. The presence of the alkyl hydrogen on the adsorbent surface which can interact with the adsorbate approve the existence of the hydrogen bonds between MG and D@DSS. C = O, C–O and –OH functional groups have been confirmed from the FTIR analysis. A summary of the dye uptake process is shown in (Fig. S3 Supplementary information).

3.13 Real Wastewater Test

To test the efficiency of D@DSS in real industrial applications, the adsorption of a wastewater effluent containing MG was performed. The composition of the industrial wastewater before performing the test is presented in Table S2, Supplementary information The adsorption studies were performed using 100 mL of industrial water, containing 10 mg L^{-1} and 50 mg L^{-1} of MG at initial pH, in the presence of 0, 7 g of D@DSS, at 50 °C at a reaction time of 80 min. As shown in Fig. 5A, the post-treatment measurement shows that 89% and 94% of MG is adsorbed for 10 mg L^{-1} and 50 mg L^{-1}, respectively. Furthermore, the removal rate is decreased when comparing the synthetic and real wastewater solutions, which is expected, especially since the real wastewater solution contains several other elements that cause the competition between MG and other existing cations in the solution. This was in correlation with the above-mentioned study of the salt effect in Fig. 3E.

3.14 Comparison of D@DSS on Adsorption

D@DSS was used for the adsorption of MG, Methylene Blue (MB) and Red Congo (RC) from aqueous mediums (Fig. 5B) to study the efficiency of the adsorbent, three dyes MG, MB, and RC (50 mg L^{-1}) with various surface charge

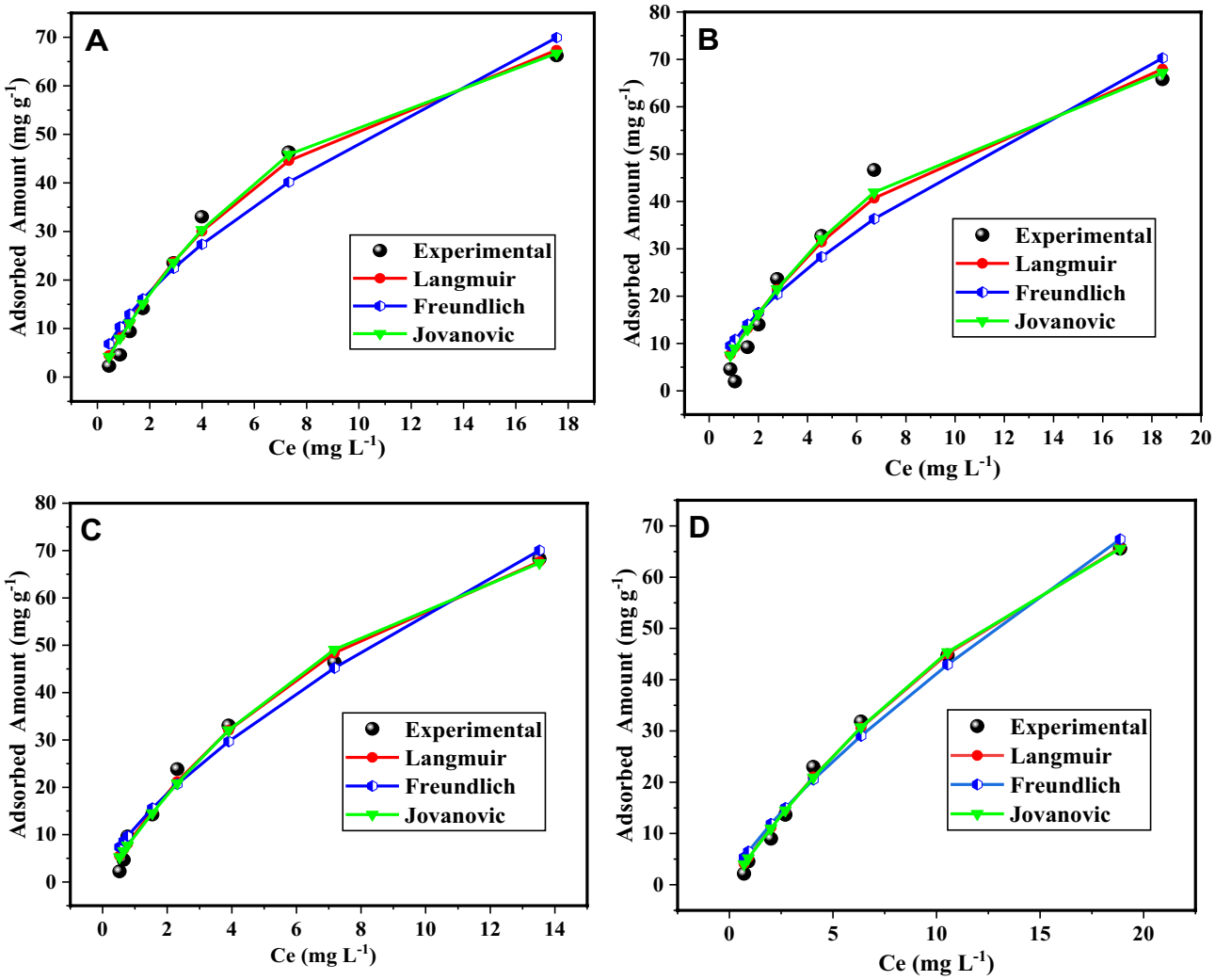

Fig. 4 Comparison between the experimental and predicted isotherms for the adsorption of MG by D@DSS adsorbent **A** at 20 °C, **B** at 30 °C, **C** at 40 °C, **D** at 50 °C

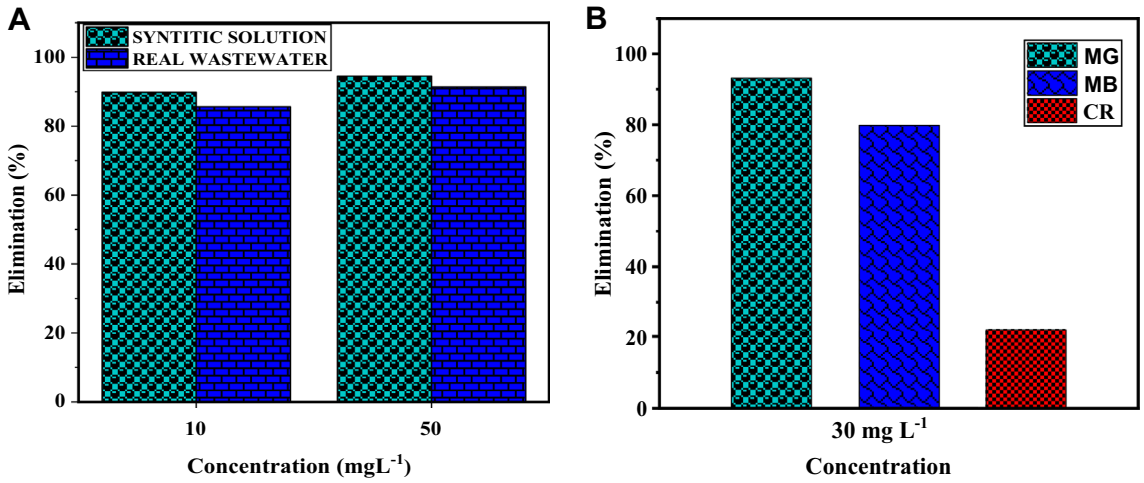

Fig. 5 **A** Histograms of the MG elimination % onto D@DSS in synthetic wastewater and real wastewater **B** histogram of the Elimination% of three different dyes into D@DSS

Table 8 Maximum adsorption capacity, of various adsorbents for MG adsorption

Adsorbents	q_m (mg g^{-1})	T (°C)	Isotherm model	S_{BET} ($m^2.g^{-1}$)	Ref.
polydopamine microspheres	151.52	45	Langmuir	Not reported	[48]
Coco-peat	19.2	40	Sips	Not reported	[26]
Mg–Al-LDH	44.44	60	Freundlich	23.150	[49]
Mg–Al/Biochar	70.92	60	Freundlich	111.404	[49]
C–Zn–Al LDH	126.58	–	Langmuir	4.554	[50]
NRH	18.1	60	Langmuir	330	[51]
Pineapple leaf powder	54.64	25	Langmuir	5.2	[52]
Bivalve shell-*Zea mays* L husk leaf	81.5	30	Langmuir	Not reported	[53]
D@DSS ($q_{m,ex}$ = 66.22 mg g^{-1})	73.93	20	Jovanovic	24, 42	This work
D@DSS ($q_{m,ex}$ = 65.78 mg g^{-1})	75.15	30	Jovanovic		
D@DSS ($q_{m,ex}$ = 68.23 mg g^{-1})	82.12	40	Jovanovic		
D@DSS ($q_{m,ex}$ = 65.56 mg g^{-1})	96.4	50	Jovanovic		

and structure properties were adsorbed using D@DDS. In the case of MG, removal percentage was 93.2%, due to strong electrostatic interaction between MG cation dye and D@DSS surface. Similarly, for MB, the percentage removal was 79, 81%. Even though D@DSS contains some functional groups such as (C=O) of carbonyl groups and silica, Si–O–Si bonds on surface are enhanced the number of active sites. For this, the D@DSS exhibited a higher and faster adsorption capability to remove a positively charged dye, for Red Congo (RC), from water under the same condition using D@DSS. The adsorption efficiency was moderate (22.1%), but less than the cationic dyes, thanks to the electrostatic repulsion between the electron-rich D@DSS surface and RC dye. In addition, the adsorption study results showed that the adsorption was possible just for pH 2 for RC removal.

Table 8 summarizes the maximum adsorption capacity values reported for other adsorbents in the literature, compared to the D@DSS adsorbent used in this study. Comparing previously reported adsorbents with the results obtained in this work, the D@DSS can be employed as a low-cost adsorbent and considered as an alternative to other materials for MG removal. Keeping in mind that the values of K_L and 1/n are in between 0 and 1 indicating that the adsorption of MG onto D@DSS adsorbent is favorable.

4 Conclusions

To conclude, the D@DSS used in this study to remove the MG shows the effectiveness of this material towards the discoloration of aqueous media contaminated by cationic dyes. Thermodynamic analysis, adsorption kinetic studies, and adsorption isotherms were carried out to clarify the mode of fixation of MG as a model cationic dye on the tested material. The D@DSS demonstrated the efficiency of adsorbing MG with a high percentage of discoloration in basic solutions (up to 97%). The PSO kinetic model applies well in the case of the studied adsorbent/adsorbate systems. The adsorption isotherms are described satisfactorily by the Jovanovic model. The maximum adsorption capacity of MG is 96 mg g^{-1} at 50 °C. The influence of NaCl salt is practically clear on the adsorption capacity. The study of the effect of temperature on the adsorption of this dye, generally shows an increase in discoloration with increasing temperature. The calculation of thermodynamic parameters shows that the adsorption process is exothermic and spontaneous. The high values of the heat of adsorption confirm that the interaction between the two supports and the dyes are of chemical nature. The studied adsorbent demonstrated a great potential to be extended to other dyes removal. Studies continue to look for less expensive carriers to be combined with the sludge to improve the depolarization efficiency for possible use in textile and other organic pollutant-loaded effluents.

Supplementary Information The online version contains supplementary material available at https://doi.org/10.1007/s42250-021-00308-x.

Acknowledgements The research work was supported by Ministry of Energy, and Mines and the Environment within the Research Project with grant number 018-1212-00019. We would like also to thank Dr. Youness Abdellaoui for his comments and revision of our manuscript. The authors would like also to thank the CAC of Cadi Ayad University of Marrakech for this support to this project.

Declarations

Conflict of interest The authors declare that there is no conflict of interest.

References

1. Ahmad R, Kumar R (2010) Adsorption studies of hazardous malachite green onto treated ginger waste. J Environ Manag 91(4):1032–1038. https://doi.org/10.1016/j.jenvman.2009.12.016
2. Khawaja H, Zahir E, Asghar MA, Asghar MA (2021) Graphene oxide decorated with cellulose and copper nanoparticle as an

efficient adsorbent for the removal of malachite green. Int J Biol Macromol 167:23–34. https://doi.org/10.1016/j.ijbiomac.2020.11.137
3. Rigueto CVT, Alessandretti I, da Silva DH, Rosseto M, Loss RA, Geraldi CAQ (2021) Agroindustrial Wastes of banana pseudostem as adsorbent of textile dye: characterization, kinetic, and equilibrium studies. Chem Afr. https://doi.org/10.1007/s42250-021-00263-7
4. Loum J, Byamukama R, Wanyama PAG (2021) Efficient extraction of natural dyes from selected plant species. Chem Afr 4(3):677–689. https://doi.org/10.1007/s42250-021-00248-6
5. Guenfoud F, Mokhtari M, Akrout H (2014) Electrochemical degradation of malachite green with BDD electrodes: effect of electrochemical parameters. Diam Relat Mater 46:8–14. https://doi.org/10.1016/j.diamond.2014.04.003
6. Wang S, Huang Y, Meng X, Liu X (2020) Highly efficient and heterogeneous OMS-2 for the directly oxidative degradation of organic dyes under acidic condition. Inorg Chem Commun 117:107969. https://doi.org/10.1016/j.inoche.2020.107969
7. Al Kausor M, Chakrabortty D (2021) Graphene oxide based semiconductor photocatalysts for degradation of organic dye in waste water: a review on fabrication, performance enhancement and challenges. Inorg Chem Commun 129:108630. https://doi.org/10.1016/j.inoche.2021.108630
8. Kavci E (2020) Malachite green adsorption onto modified pine cone: Isotherms, kinetics and thermodynamics mechanism. Chem Eng Commun. https://doi.org/10.1080/00986445.2020.1715961
9. Dabagh A, Bagui A, Abali M, Aziam R, Chiban M, Sinan F, Zerbet M (2021) Increasing the adsorption efficiency of methylene blue by acid treatment of the plant *Carpobrotus edulis*. Chem Afr 4(3):585–598. https://doi.org/10.1007/s42250-021-00233-z
10. El-Bindary MA, El-Desouky MG, El-Bindary AA (2021) Adsorption of industrial dye from aqueous solutions onto thermally treated green adsorbent: a complete batch system evaluation. J Mol Liq. https://doi.org/10.1016/j.molliq.2021.117082
11. Djilani C, Zaghdoudi R, Djazi F, Bouchekima B, Lallam A, Modarressi A, Rogalski M (2015) Adsorption of dyes on activated carbon prepared from apricot stones and commercial activated carbon. J Taiwan Inst Chem Eng 53:112–121. https://doi.org/10.1016/j.jtice.2015.02.025
12. Azeez L, Adejumo AL, Asaolu SS, Adeoye MD, Adetoro RO (2020) Functionalization of rice husks with ortho-phosphoric acid enhanced adsorptive capacity for anionic dye removal. Chem Afr. https://doi.org/10.1007/s42250-020-00142-7
13. Rafatullah M, Sulaiman O, Hashim R, Ahmad A (2010) Adsorption of methylene blue on low-cost adsorbents: a review. J Hazard Mater 177(1–3):70–80. https://doi.org/10.1016/j.jhazmat.2009.12.047
14. Bushra R, Mohamad S, Alias Y, Jin Y, Ahmad M (2021) Current approaches and methodologies to explore the perceptive adsorption mechanism of dyes on low-cost agricultural waste: a review. Microporous Mesoporous Mater 319:111040. https://doi.org/10.1016/j.micromeso.2021.111040
15. Chowdhury S, Saha P (2010) Sea shell powder as a new adsorbent to remove Basic Green 4 (Malachite Green) from aqueous solutions: equilibrium, kinetic and thermodynamic studies. Chem Eng J 164(1):168–177. https://doi.org/10.1016/j.cej.2010.08.050
16. Chowdhury S, Mishra R, Saha P, Kushwaha P (2011) Adsorption thermodynamics, kinetics and isosteric heat of adsorption of malachite green onto chemically modified rice husk. Desalination 265(1–3):159–168. https://doi.org/10.1016/j.desal.2010.07.047
17. Magriotis ZM, Carvalho MZ, de Sales PF, Alves FC, Resende RF, Saczk AA (2014) Castor bean (*Ricinus communis* L.) presscake from biodiesel production: an efficient low cost adsorbent for removal of textile dyes. J Environ Chem Eng 2(3):1731–1740. https://doi.org/10.1016/j.jece.2014.07.005
18. Kazemi SY, Biparva P, Ashtiani E (2016) Cerastoderma lamarcki shell as a natural, low cost and new adsorbent to removal of dye pollutant from aqueous solutions: equilibrium and kinetic studies. Ecol Eng 88:82–89. https://doi.org/10.1016/j.ecoleng.2015.12.020
19. Lee S-L, Park J-H, Kim S-H, Kang S-W, Cho J-S, Jeon J-R, Seo D-C (2019) Sorption behavior of malachite green onto pristine lignin to evaluate the possibility as a dye adsorbent by lignin. Appl Biol Chem. https://doi.org/10.1186/s13765-019-0444-2
20. Cheng W, Wang S-G, Lu L, Gong W-X, Liu X-W, Gao B-Y, Zhang H-Y (2008) Removal of malachite green (MG) from aqueous solutions by native and heat-treated anaerobic granular sludge. Biochem Eng J 39(3):538–546. https://doi.org/10.1016/j.bej.2007.10.016
21. Aoulad El Hadj Ali Y, Ahrouch M, Ait Lahcen A, Demba N'diaye A, El Yousfi F, Stitou M (2021) Dried sewage sludge as an efficient adsorbent for pollutants: cationic methylene blue removal case study. Nanotechnol Environ Eng. https://doi.org/10.1007/s41204-021-00111-6
22. Langmuir I (1916) The constitution and fundamental properties of solids and liquids. J Am Chem Soc 38:2221–2295
23. Ho Y (2006) Review of second-order models for adsorption systems. J Hazard Mater 136(3):681–689. https://doi.org/10.1016/j.jhazmat.2005.12.043
24. Freundlich H. M. F. (1906) Over the adsorption in solution. J Phys Chem 57:385–471
25. Quesada-Peñate I, Julcour-Lebigue C, Jáuregui-Haza U-J, Wilhelm A-M, Delmas H (2009) Comparative adsorption of levodopa from aqueous solution on different activated carbons. Chem Eng J 152(1):183–188. https://doi.org/10.1016/j.cej.2009.04.039
26. Vijayaraghavan K, Premkumar Y, Jegan J (2015) Malachite green and crystal violet biosorption onto coco-peat: characterization and removal studies. Desalin Water Treat 57(14):6423–6431. https://doi.org/10.1080/19443994.2015.1011709
27. Hajialigol S, Masoum S (2019) Optimization of biosorption potential of nano biomass derived from walnut shell for the removal of Malachite Green from liquids solution: experimental design approaches. J Mol Liq 286:110904. https://doi.org/10.1016/j.molliq.2019.110904
28. Jalilvand P, Rahbar-Kelishami A, Mohammadi T, Shayesteh H (2020) Optimizing of malachite green extraction from aqueous solutions using hydrophilic and hydrophobic nanoparticles. J Mol Liq. https://doi.org/10.1016/j.molliq.2020.113014
29. Myers RH, Montgomery DC, Vining GG, Borror CM, Kowalski SM (2004) Response surface methodology: a retrospective and literature survey. J Qual Technol 36(1):53–77. https://doi.org/10.1080/00224065.2004.11980
30. Garg UK, Kaur MP, Garg VK, Sud D (2008) Removal of Nickel(II) from aqueous solution by adsorption on agricultural waste biomass using a response surface methodological approach. Biores Technol 99(5):1325–1331. https://doi.org/10.1016/j.biortech.2007.02.011
31. Shaoqing Y, Jun H, Jianlong W (2010) Radiation-induced catalytic degradation of p-nitrophenol (PNP) in the presence of TiO_2 nanoparticles. Radiat Phys Chem 79(10):1039–1046. https://doi.org/10.1016/j.radphyschem.2010.05.008
32. N'diaye AD, Aoulad El Hadj Ali Y, Ould El Moustapha A (2020) Sorption of malachite green from aqueous solution using typha australis leaves as a low cost sorbent. J Environ Treat Technol 8(3):1023–1028
33. Mohanta J, Kumari R, Dey B, Dey S (2020) Highly porous iron–zirconium–zinc ternary metal oxide scaffold: facile synthesis and efficient removal of malachite green from water. J Chem Eng Data 66(1):297–307. https://doi.org/10.1021/acs.jced.0c00681
34. Mohanta J, Dey B, Dey S (2020) Sucrose-triggered, self-sustained combustive synthesis of magnetic nickel oxide nanoparticles and

efficient removal of malachite green from water. ACS Omega. https://doi.org/10.1021/acsomega.0c00999
35. Billah REK, Abdellaoui Y, Anfar Z, Giácoman-Vallejos G, Agunaou M, Soufiane A (2020) Synthesis and characterization of chitosan/fluorapatite composites for the removal of Cr(VI) from aqueous solutions and optimized parameters. Water Air Soil Pollut. https://doi.org/10.1007/s11270-020-04535-9
36. Parthasarathy P, Manju N, Hema M, Arivoli S (2011) Removal of malachite green from industrial waste-water by activated carbon prepared from cashew nut bark. Alfa Univ 2(2):41–54
37. Guechi E-K, Hamdaoui O (2013) Cattail leaves as a novel biosorbent for the removal of malachite green from liquid phase: data analysis by non-linear technique. Desalin Water Treat 51(16–18):3371–3380. https://doi.org/10.1080/19443994.2012.74919
38. Khattri SD, Singh MK (2009) Removal of malachite green from dye wastewater using neem sawdust by adsorption. J Hazard Mater 167(1–3):1089–1094. https://doi.org/10.1016/j.jhazmat.2009.01.101
39. Akar E, Altinişik A, Seki Y (2013) Using of activated carbon produced from spent tea leaves for the removal of malachite green from aqueous solution. Ecol Eng 52:19–27. https://doi.org/10.1016/j.ecoleng.2012.12.032
40. Bhagavathi Pushpa T, Vijayaraghavan J, Sardhar Basha SJ, Sekaran V, Vijayaraghavan K, Jegan J (2015) Investigation on removal of malachite green using EM based compost as adsorbent. Ecotoxicol Environ Saf 118:177–182. https://doi.org/10.1016/j.ecoenv.2015.04.033
41. Lima EC, Hosseini-Bandegharaei A, Moreno-Piraján JC, Anastopoulos I (2018) A critical review of the estimation of the thermodynamic parameters on adsorption equilibria. Wrong use of equilibrium constant in the Van't Hoof equation for calculation of thermodynamic parameters of adsorption. J Mol Liq. https://doi.org/10.1016/j.molliq.2018.10.048
42. Ahrouch M, Gatica JM, Draoui K, Vidal H (2019) Adding value to natural clays as low-cost adsorbents of methylene blue in polluted water through honeycomb monoliths manufacture. SN Appl Sci. https://doi.org/10.1007/s42452-019-1636-4
43. Lima EC, Hosseini-Bandegharaei A (2019) Response to some remarks on a critical review of the estimation of the thermodynamic parameters on adsorption equilibria. Wrong use of equilibrium constant in the van't Hoff equation for calculation of thermodynamic parameters of adsorption. J Mol Liq. 273:425–434
44. Abdellaoui Y, El Ibrahimi B, Abou Oualid H, Kassab Z, Quintal-Franco C, Giácoman-Vallejos G, Gamero-Melo P (2021) Iron-zirconium microwave-assisted modification of small-pore zeolite W and its alginate composites for enhanced aqueous removal of As(V) ions: experimental and theoretical studies. Chem Eng J 421:129909. https://doi.org/10.1016/j.cej.2021.129909
45. Sartape AS, Mandhare AM, Jadhav VV, Raut PD, Anuse MA, Kolekar SS (2017) Removal of malachite green dye from aqueous solution with adsorption technique using *Limonia acidissima* (wood apple) shell as low cost adsorbent. Arab J Chem 10:S3229–S3238. https://doi.org/10.1016/j.arabjc.2013.12.019
46. Aniagor CO, Igwegbe CA, Ighalo JO, Oba SN (2021) Adsorption of doxycycline from aqueous media: a review. J Mol Liq 334:116124. https://doi.org/10.1016/j.molliq.2021.116124
47. Oba SN, Ighalo JO, Aniagor CO, Igwegbe CA (2021) Removal of ibuprofen from aqueous media by adsorption: a comprehensive review. Sci Total Environ 780:146608. https://doi.org/10.1016/j.scitotenv.2021.146608
48. Fu J, Xin Q, Wu X, Chen Z, Yan Y, Liu S, Xu Q (2016) Selective adsorption and separation of organic dyes from aqueous solution on polydopamine microspheres. J Colloid Interface Sci 461:292–304. https://doi.org/10.1016/j.jcis.2015.09.017
49. Badri AF, Siregar PMSBN, Palapa NR, Mohadi R, Mardiyanto M, Lesbani A (2021) Mg-Al/biochar composite with stable structure for malachite green adsorption from aqueous solutions. Bull Chem React Eng Catal 16(1):149–160
50. George G, Saravanakumar MP (2018) Facile synthesis of carbon-coated layered double hydroxide and its comparative characterisation with Zn–Al LDH: application on crystal violet and malachite green dye adsorption—isotherm, kinetics and Box-Behnken design. Environ Sci Pollut Res. https://doi.org/10.1007/s11356-018-3001-3
51. Ramaraju B, Manoj Kumar Reddy P, Subrahmanyam C (2013) Low cost adsorbents from agricultural waste for removal of dyes. Environ Prog Sustain Energy 33(1):38–46. https://doi.org/10.1002/ep.11742
52. Chowdhury S, Chakraborty S, Saha P (2011) Biosorption of Basic Green 4 from aqueous solution by *Ananas comosus* (pineapple) leaf powder. Colloids Surf B 84(2):520–527. https://doi.org/10.1016/j.colsurfb.2011.02.009
53. Jalil AA, Triwahyono S, Yaakob MR, Azmi ZZA, Sapawe N, Kamarudin NHN, Hameed BH (2012) Utilization of bivalve shell-treated *Zea mays* L. (maize) husk leaf as a low-cost biosorbent for enhanced adsorption of malachite green. Biores Technol 120:218–224. https://doi.org/10.1016/j.biortech.2012.06.066